ARL

Doppler Processing with Ultra-Wideband (UWB) Radar Revisited

by Traian Dogaru

NOTICES

Disclaimers

The findings in this report are not to be construed as an official Department of the Army position unless so designated by other authorized documents.

Citation of manufacturer's or trade names does not constitute an official endorsement or approval of the use thereof.

Destroy this report when it is no longer needed. Do not return it to the originator.

ARL

US Army Research Laboratory

Doppler Processing with Ultra-Wideband (UWB) Radar Revisited

by Traian Dogaru
Sensors and Electron Devices Directorate, ARL

REPORT DOCUMENTATION PAGE			*Form Approved* *OMB No. 0704-0188*

Public reporting burden for this collection of information is estimated to average 1 hour per response, including the time for reviewing instructions, searching existing data sources, gathering and maintaining the data needed, and completing and reviewing the collection information. Send comments regarding this burden estimate or any other aspect of this collection of information, including suggestions for reducing the burden, to Department of Defense, Washington Headquarters Services, Directorate for Information Operations and Reports (0704-0188), 1215 Jefferson Davis Highway, Suite 1204, Arlington, VA 22202-4302. Respondents should be aware that notwithstanding any other provision of law, no person shall be subject to any penalty for failing to comply with a collection of information if it does not display a currently valid OMB control number.
PLEASE DO NOT RETURN YOUR FORM TO THE ABOVE ADDRESS.

1. REPORT DATE *(DD-MM-YYYY)* January 2018	2. REPORT TYPE Technical Note		3. DATES COVERED (From - To) December 2017
4. TITLE AND SUBTITLE Doppler Processing with Ultra-Wideband (UWB) Radar Revisited			5a. CONTRACT NUMBER
			5b. GRANT NUMBER
			5c. PROGRAM ELEMENT NUMBER
6. AUTHOR(S) Traian Dogaru			5d. PROJECT NUMBER
			5e. TASK NUMBER
			5f. WORK UNIT NUMBER
7. PERFORMING ORGANIZATION NAME(S) AND ADDRESS(ES) US Army Research Laboratory ATTN: RDRL-SER-U 2800 Power Mill Road, Adelphi, MD 20783-1138			8. PERFORMING ORGANIZATION REPORT NUMBER ARL-TN-0866
9. SPONSORING/MONITORING AGENCY NAME(S) AND ADDRESS(ES)			10. SPONSOR/MONITOR'S ACRONYM(S)
			11. SPONSOR/MONITOR'S REPORT NUMBER(S)
12. DISTRIBUTION/AVAILABILITY STATEMENT Approved for public release; distribution is unlimited.			
13. SUPPLEMENTARY NOTES			

14. ABSTRACT

This technical note revisits previous work performed at the US Army Research Laboratory related to Doppler processing in radar systems using ultra-wideband (UWB) waveforms. In light of more recent research in this area, we demonstrate that exact reconstruction of the range and Doppler profiles is possible under UWB excitation, with the same Doppler resolution as that afforded by narrowband radar systems. Detailed theoretical derivations, as well as a simple numerical example, are included. Additionally, we discuss the computational aspects of this method and analyze the range and Doppler ambiguities introduced by the new processing scheme, showing its advantage in mitigating the Doppler grating lobes as compared to the conventional Doppler processing counterpart.

15. SUBJECT TERMS

Doppler radar, UWB radar, matched filter, ambiguity function, ultra-wideband waveforms

16. SECURITY CLASSIFICATION OF:			17. LIMITATION OF ABSTRACT	18. NUMBER OF PAGES	19a. NAME OF RESPONSIBLE PERSON Traian Dogaru
a. REPORT Unclassified	b. ABSTRACT Unclassified	c. THIS PAGE Unclassified	UU	30	19b. TELEPHONE NUMBER (Include area code) 301-394-1482

Standard Form 298 (Rev. 8/98)
Prescribed by ANSI Std. Z39.18

Contents

List of Figures

1. Introduction

The ultra-wideband (UWB) radar technology has many applications to sensing scenarios where high resolution and typically low microwave frequencies are required, such as sensing through the wall, ground, or foliage penetrating radar. The US Army Research Laboratory has investigated this technology for more than 2 decades, with an emphasis on radar imaging applications.

A previous study by this author[1] suggested that UWB waveforms are not the best choice for Doppler radar processing due to the issue of target range migration during the integration interval. However, more recent investigations[2,3] have demonstrated that this problem can be overcome by the correct choice of the matched filter in the case of UWB waveforms. While the ideas, mathematical derivations, and numerical examples in this note were developed independently, they are very similar to the results already published by Le Chevalier[2] and He et al.[3] Although not entirely original, this note was written mainly as an update to the conclusions of our previous work.[1] Additionally, we include a discussion of the computational aspects of this technique as well as a detailed account of the wideband ambiguity function (AF) and related Doppler ambiguity issues, which, to our knowledge, have not been published elsewhere.

This report is organized as follows. In Section 2, we develop the theory behind the new Doppler processing technique using UWB waveforms. Section 3 presents a simple numerical example and compares the new method with the conventional Doppler processing approach. In Section 4, we discuss both the computational aspects of implementing the wideband matched filter and the issue of Doppler ambiguities in the context of the new processing scheme. We finalize with conclusions in Section 5.

2. Theoretical Description

The following symbols are used in this and the following sections:

p – complex envelope of the transmitted waveform in the time domain

P – transmitted waveform envelope spectrum (frequency domain)

x – transmitted waveform (complex form)

y – received waveform (complex form)

z – demodulated received waveform (complex form)

s – 2-D received signal in the fast time domain

S – 2-D received signal in the frequency domain

Q – phase factor in the 2-D point target response

RDM – 2-D range-Doppler map

t – time (in general)

t_f – fast time

t_s – slow time

T_r – pulse repetition interval

T_{CPI} – coherent processing interval

τ – received waveform delay

r – target range

R – target range in the middle of the coherent processing interval (CPI)

f – RF frequency (Fourier pair of fast time)

f_0 – carrier frequency

f_d – Doppler frequency

B – pulse bandwidth

v – radial velocity of the target

c – speed of light

ρ – variable representing the Fourier pair of range (R)

u – variable representing the Fourier pair of velocity

δf_d – Doppler frequency resolution

δv – velocity resolution

δR – range resolution

Typically, Doppler processing in radar consists of creating range-Doppler (R/D) maps—these are 2-D reflectivity maps of the scene under investigation by the radar sensor, plotted as a function of the range and radial velocity (or, equivalently, Doppler frequency) dimensions. The creation of the R/D map can be seen as the application of a matched filter along these 2 dimensions. To determine the equation governing this matched filter, we need to derive the radar response of a point target.

Assume that a point target is moving with constant radial velocity v toward the radar during a CPI. Then, its range varies as $r(t) = R - vt$, where R is the range in the middle of the CPI and t runs from $-\dfrac{T_{CPI}}{2}$ to $\dfrac{T_{CPI}}{2}$. Also, assume that the transmitted waveform consists of a train of N short UWB impulses with complex envelope $p(t)$ and carrier frequency f_0, with a repetition interval T_r:

$$x(t) = \sum_{n=0}^{N-1} p(t - nT_r)\exp(j2\pi f_0 t). \tag{1}$$

The signal received from the point target considered previously is proportional to a delayed version of the transmitted signal, up to a complex constant factor. We write the received signal as

$$y_{PT}(t) = x\left(t - \frac{2r(t)}{c}\right) = \sum_{n=0}^{N-1} p\left(t - nT_r - \frac{2R}{c} + \frac{2v}{c}t\right)\exp\left(j2\pi f_0\left(t - \frac{2R}{c} + \frac{2v}{c}t\right)\right). \tag{2}$$

Note that throughout this note, we work with complex analytic signals, meaning we consider both the in-phase and quadrature (I–Q) signal components. Upon down-conversion to baseband, we eliminate the factor $\exp(j2\pi f_0 t)$ and obtain

$$z_{PT}(t) = \sum_{n=0}^{N-1} p\left(t - nT_r - \frac{2R}{c} + \frac{2v}{c}t\right)\exp\left(j\left(-\frac{4\pi f_0 R}{c} + \frac{4\pi f_0}{c}vt\right)\right). \tag{3}$$

At this point, we need to mention that this theoretical derivation is valid for any type of UWB waveforms, not only short impulses as considered in Eq. 1. When pulse compression waveforms are used for this purpose, $p(t)$ represents the pulse envelope obtained after compressing the received signal.

The signal $z(t)$ is sampled in the time variable, and its samples $z(t_k)$ are rearranged in a 2-D array indexed by the discrete variables $t_{fm} = t_k - nT_r$ (fast time) and $t_{sn} = nT_r$ (slow time; note that the radar waveform is already discretized along this dimension by its pulsed nature). When denoting the new 2-D signal $s(t_{fm}, t_{sn})$ returned by a point target at range R and moving with velocity v, we add the arguments R and v to its description:

$$s_{PT}\left(t_{fm}, t_{sn}, R, v\right)$$

$$= p\left(t_{fm} - \frac{2R}{c} + \frac{2v}{c}\left(t_{fm} + t_{sn}\right)\right)\exp\left(j\left(-\frac{4\pi f_0}{c}R + \frac{4\pi f_0}{c}v\left(t_{fm} + t_{sn}\right)\right)\right), \quad (4)$$

$$\cong p\left(t_{fm} - \frac{2R}{c} + \frac{2v}{c}t_{sn}\right)\exp\left(j\left(-\frac{4\pi f_0}{c}R + \frac{4\pi f_0}{c}vt_{sn}\right)\right)$$

with $m = 0, \ldots M - 1$ and $n = -\frac{N}{2}, \ldots \frac{N}{2} - 1$. In the last equation, we neglected t_{fm} whenever it appeared together with t_{sn} inside the same factor, since $t_{fm} \ll t_{sn}$, which amounts to saying that the pulse width of $p(t)$ is assumed much smaller than the repetition interval T_r. Note the strong similarity between this equation and Eq. 11 in our previous note,[1] where a Gaussian envelope was chosen for the transmitted pulse. Let us take the discrete Fourier transform (DFT) of s_{PT} along the t_{fm} dimension, whose Fourier variable pair is the discrete frequency f_m:

$$S_{PT}\left(f_m, t_{sn}, R, v\right) = P\left(f_m\right)\exp\left(j\left(-\frac{4\pi\left(f_m + f_0\right)R}{c} + \frac{4\pi\left(f_m + f_0\right)vt_{sn}}{c}\right)\right), \quad (5)$$

$$= P\left(f_m\right)Q\left(f_m, t_{sn}, R, v\right)$$

where $f_m = m\frac{B}{M}$, with $m = \frac{M}{2}, \ldots \frac{M}{2} - 1$, and $P(f)$ is the spectrum of $p(t)$. $P(f)$ is typically a real-valued function; this is the case when $p(t)$ is a symmetric pulse envelope as well as when $p(t)$ is obtained by compression of the original transmitted waveform.

The transfer function of the matched filter is designed to compensate the phase of the response of a point target at range R and moving with velocity v. Therefore, assuming $P(f)$ is real, the matched filter transfer function is $Q^*\left(f_m, t_{sn}, R, v\right)$. The R/D map, which represents the output of the matched filter for the pair of coordinates (R, v) and the input $S\left(f_m, t_{sn}\right)$ (the response of an arbitrary scene), can be expressed as

$$RDM\left(R, v\right) = \sum_{m=0}^{M-1}\sum_{n=0}^{N-1} S\left(f_m, t_{sn}\right)Q^*\left(f_m, t_{sn}, R, v\right)$$

$$= \sum_{m=0}^{M-1}\sum_{n=0}^{N-1} S\left(f_m, t_{sn}\right)\exp\left(j\left(\frac{4\pi\left(f_m + f_0\right)R}{c} - \frac{4\pi\left(f_m + f_0\right)vt_{sn}}{c}\right)\right). \quad (6)$$

Before we take a more in-depth look at Eq. 6, we compare this formula to that obtained by conventional Doppler processing (as considered in our previous work[1]). Starting again with the $S(f_m, t_{sn})$ 2-D signal, the R/D map in conventional Doppler processing is obtained according to

$$RDM_C(R,v) = \sum_{m=0}^{M-1}\sum_{n=0}^{N-1} S(f_m, t_{sn}) \exp\left(j\left(\frac{4\pi f_m R}{c} - \frac{4\pi f_0 v t_{sn}}{c} \right) \right). \tag{7}$$

Equation 7 can be clearly interpreted as a 2-D DFT[4] of the $S(f_m, t_{sn})$ signal. (Although R and v are formally written as continuous variables in our equations, they always take on discrete values in a practical implementation.) Thus, the sum over m amounts to a DFT along the frequency-range dimension, while the sum over n amounts to a DFT along the slow time-velocity dimension. The additional phase factor $\exp\left(j\frac{4\pi f_0 R}{c} \right)$ appearing in Eq. 6 is unimportant and was simply included to make the formula more symmetric. However, the factor $\exp\left(-j\frac{4\pi f_m t_{sn}}{c} \right)$, which is missing from Eq. 7, is critical for Doppler processing with UWB waveforms. Its omission from Eq. 7 means that the matched filter fails to compensate for the corresponding factor present in Eq. 5 and explains the R/D map artifacts for the method described in our previous work.[1] Notice that neglecting this phase factor is well justified in the case of narrowband signals, where $f_m \ll f_0$; however, this approximation is not valid for UWB waveforms, where f_m and f_0 are of the same order of magnitude.

It is also interesting to rewrite the formula in Eq. 6 as a function of the delay (τ) and Doppler frequency (f_d) variables, which are connected to R and v by $\tau = \frac{2R}{c}$ and $f_d = \frac{2f_0}{c}v$, respectively.

$$RDM(\tau, f_d) = \sum_{m=0}^{M-1}\sum_{n=0}^{N-1} S(f_m, t_{sn}) \exp\left(j2\pi\left((f_m + f_0)\tau - \left(1 + \frac{f_m}{f_0}\right)f_d t_{sn} \right) \right). \tag{8}$$

Going back to Eq. 6, we introduce the new variables $\rho_m = \frac{2(f_m + f_0)}{c}$ and $u_{m,n} = -\frac{2(f_m + f_0)t_{sn}}{c}$ and rewrite the R/D map formula as

$$RDM(R,v) = \sum_{m=0}^{M-1}\sum_{n=0}^{N-1} S(\rho_m, u_{m,n}) \exp(j2\pi(\rho_m R + u_{m,n}v)). \tag{9}$$

The last equation is reminiscent of a 2-D DFT of the signal $S(\rho_m, u_{m,n})$, involving the Fourier variable pairs (ρ, R) and (u, v). However, when the frequency and slow time variables are sampled on a regular rectangular grid (at equal intervals in both dimensions), the samples of ρ and u cover a wedge-shaped domain in the $\rho - u$ plane, as illustrated in Fig. 1. As a consequence, we cannot apply efficient algorithms, such as the 2-D fast Fourier transform (FFT), to directly compute the expression in Eq. 9; instead, we need to apply a brute-force approach to evaluate Eq. 9. A further discussion of the computational aspects of this procedure is offered in Section 4.1.
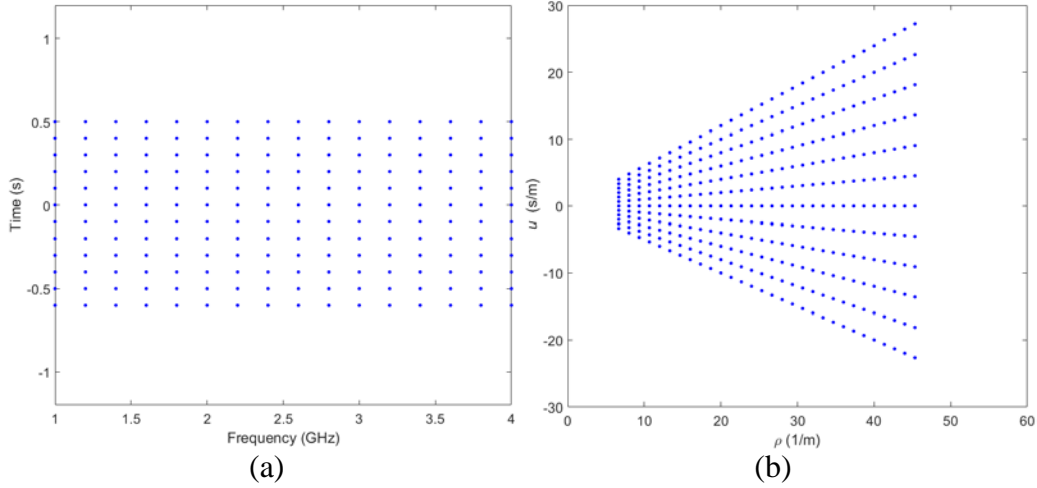

(a)   (b)

Fig. 1   Sample points used in creating R/D maps by the matched filter method, illustrating the radar data support in (a) the frequency-slow time domain and (b) the ρ-u domain. The samples correspond to the numerical example in Section 3, down-sampled for figure clarity.

A computationally efficient processing scheme for the implementation of Eq. 9, which takes advantage of the 2-D FFT algorithm, can be obtained using the Keystone transform.[3] This consists of remapping the radar data samples from their original format (rectangular in the $f - t_s$ plane) onto a new grid such that the resulting samples in the $\rho - u$ plane have a rectangular support. The formula describing the coordinate transformation in the $f - t_s$ plane is

$$t_s' = \frac{f + f_0}{f_0} t_s = \frac{c}{2f_0} u. \tag{10}$$

When replotted in the $f - t_s'$ coordinates, the radar data samples are arranged in the pattern shown in Fig. 2a. Correspondingly, the new data support in the $\rho - u$ plane

takes on a rectangular shape (Fig. 2b), which allows the application of the 2-D FFT to compute the expression in Eq. 9. An intermediate step consisting of interpolating the radar data from the $f - t_s$ to the $f - t_s'$ coordinates is required by this method.
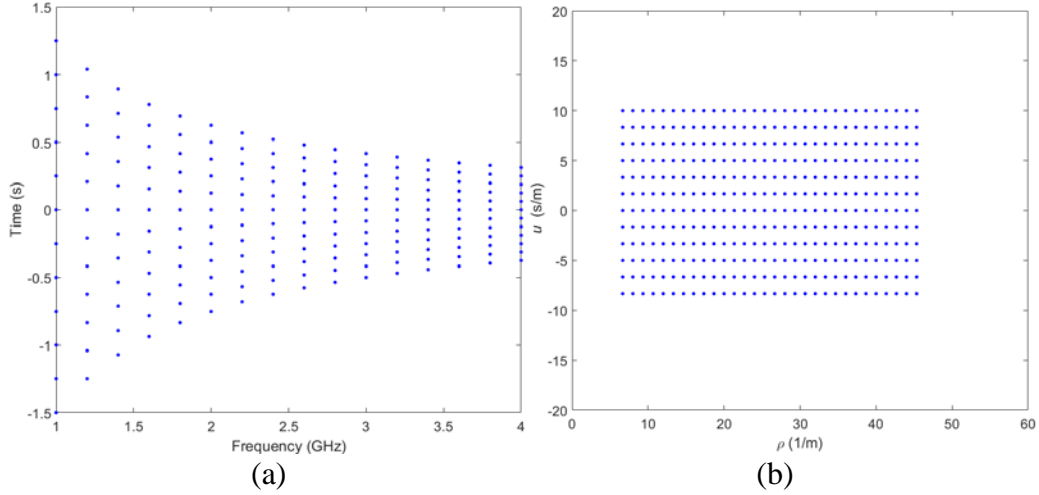

(a) (b)

Fig. 2   Sample points used in creating R/D maps by the Keystone transform method, illustrating the radar data support in (a) the frequency-slow time domain and (b) the ρ-u domain. The samples correspond to the numerical example in Section 3, down-sampled for figure clarity.

With regard to the resolution of this radar data-processing approach, the same formulas as for conventional, narrowband Doppler processing apply. Thus, the range, Doppler frequency, and velocity resolutions are, respectively:

$$\delta R = \frac{c}{2B}, \tag{11a}$$

$$\delta f_d = \frac{1}{T_{CPI}}, \text{ and} \tag{11b}$$

$$\delta v = \frac{c}{2T_{CPI} f_0}. \tag{11c}$$

All these resolution formulas are approximate and do not account for possible windowing of the radar data in the frequency and slow time domains. The formulas in Eqs. 11b and 11c assume that the slow time interval covered by the radar samples at f_0 is T_{CPI}. Importantly, the resolution in both dimensions (R and v) is uniform over the entire R/D space, unlike the processing scheme in our previous work.[1]

Before concluding this section, we should mention that the Doppler processing with UWB pulses described in this note is just another example of multidimensional

signal processing encountered in radar applications. Particularly, we can draw a parallel with the formation of wideband, widebeam synthetic aperture radar (SAR) images, where a similar coupling between the 2 dimensions of the radar data space (frequency and aperture position) requires the application of a 2-D matched filter. The conventional Doppler processing is analogous to the Doppler beam sharpening[5] method in SAR imaging, which is known to produce significant artifacts when used in conjunction with UWB signals and wide angle apertures. The brute-force matched filter for R/D maps described by Eq. 6 corresponds to the matched filter method for SAR image formation, which is the frequency-domain version of the popular backprojection algorithm.[5] On the other hand, the Keystone transform method corresponds to the range migration algorithm for SAR image formation,[6] which uses the Stolt interpolation to remap the data samples from the original wedge-shaped support in the $k_x - k_y$ plane to a rectangular grid, followed by the application of a 2-D FFT (note that the Stolt transform formula differs from the Keystone transform due to different sensing geometries and radar data dimensions, but the principle of the 2 methods is very similar).

3. Numerical Example

We present a numerical example to illustrate the processing scheme developed in the previous section by a simple simulation. Consider 2 point targets moving with radial velocities $v_1 = 0.4$ m/s and $v_2 = -0.6$ m/s (positive v indicates a target moving *toward* the radar), with initial ranges $R_{01} = 4.05$ m and $R_{02} = 3.3$ m. The radar transmits a train of modulated Gaussian pulses[1] with the envelope $p(t) = \exp\left(-\dfrac{t^2}{\tau_0^2}\right)$. The pulse width is $\tau_0 = 500$ ps (which corresponds to a bandwidth of approximately 2 GHz) and the carrier frequency is $f_0 = 2.5$ GHz. An illustration of the individual pulse in the time and frequency domains is shown in Fig. 3.

The pulse repetition interval is $T_r = 25$ ms, which corresponds to a pulse repetition frequency (PRF) of 40 Hz. The CPI has a duration $T_{CPI} = 1.2$ s and involves the coherent processing of $N = 48$ pulses. The total observation interval is 3 s. A representation of the radar data returned by the targets as a function of range and slow time is shown in Fig. 4. In the subsequent processing examples, we create a single R/D map corresponding to a CPI centered at $t = 1.5$ s, with the targets at ranges $R_1 = R_{01} - v_1 t = 3.45$ m and $R_2 = R_{02} - v_2 t = 4.2$ m, in the middle of the CPI. The unambiguous velocity interval covered by this processing scheme runs from –1.2 to 1.2 m/s.
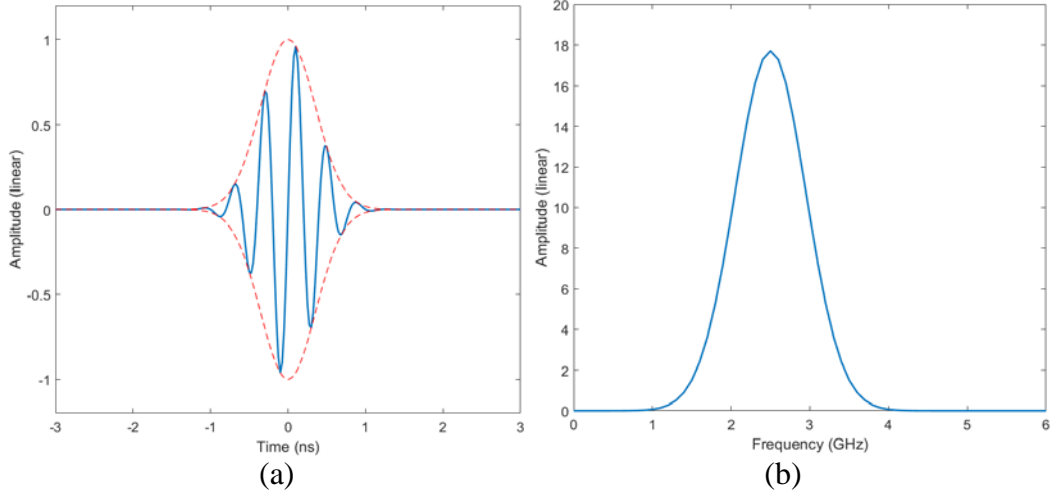
Fig. 3 **Representation of the modulated Gaussian UWB impulse used as excitation in the numerical example, in (a) the time domain and (b) the frequency domain. The red dotted lines represent the pulse envelope.**
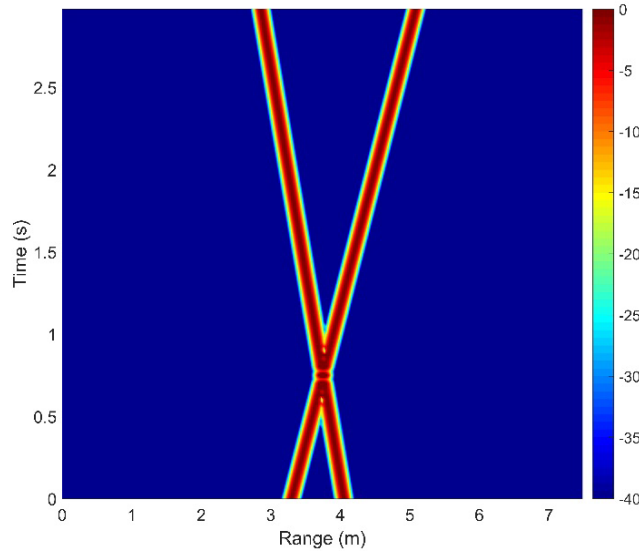

Fig. 4 **Representation of the radar-received data in the range-slow time domain, showing the 2 targets considered in the numerical example**

Each received waveform within a repetition interval is discretized into $M = 300$ fast time samples, using a time step $\Delta t = 167 \text{ ps}$. The total fast time interval covered by these samples is 50 ns, which corresponds to a target range running from 0 to 7.5 m. The frequency-domain increment is 20 MHz, covering 6 GHz of bandwidth (from 1 to 7 GHz). However, since the processing scheme uses I–Q data in the fast time domain, only the first half of the spectrum (from 1 to 4 GHz) contains nonzero data samples. Note that the frequency offset (f_m in Eq. 6) runs from –1.5 to 4.5 GHz, although only data corresponding to frequency offsets from –1.5 to 1.5 GHz contribute to the sum over m.

To mitigate the sidelobes in the R/D maps, we use the original Gaussian frequency-domain window of the transmitted pulse (for range sidelobe suppression) and a Hanning slow time domain window (for Doppler sidelobe suppression).

In Figs. 5–7 we present the R/D map obtained for the CPI centered at 1.5 s using 3 different processing schemes: 1) conventional Doppler processing, corresponding to Eq. 7 (Fig. 5); 2) the direct implementation of the matched filter described by Eq. 6 (Fig. 6); and 3) the matched filter implemented via the Keystone transform method (Fig. 7). The target images in Fig. 5 illustrate the main issues with conventional Doppler processing applied to UWB radar: poor resolution in both range and Doppler, which degrades even further with increasing target velocity. On the other hand, Figs. 6 and 7 demonstrate that careful implementation of the R/D matched filter for UWB radar can reach the same Doppler resolution limit as a narrowband radar system, independent of the target velocity. The only difference between the target images in Figs. 6 and 7 consists of the sidelobe directions, which cannot be distinguished in the R/D maps due to the limited dynamic range.

Fig. 5 **R/D map of the 2 targets considered in the numerical example, obtained by conventional Doppler processing, for a 1.2-s CPI centered at** $t = 1.5$ **s**

Fig. 6   **R/D map of the 2 targets considered in the numerical example, obtained by the matched filter method, for a 1.2-s CPI centered at** t **= 1.5 s**
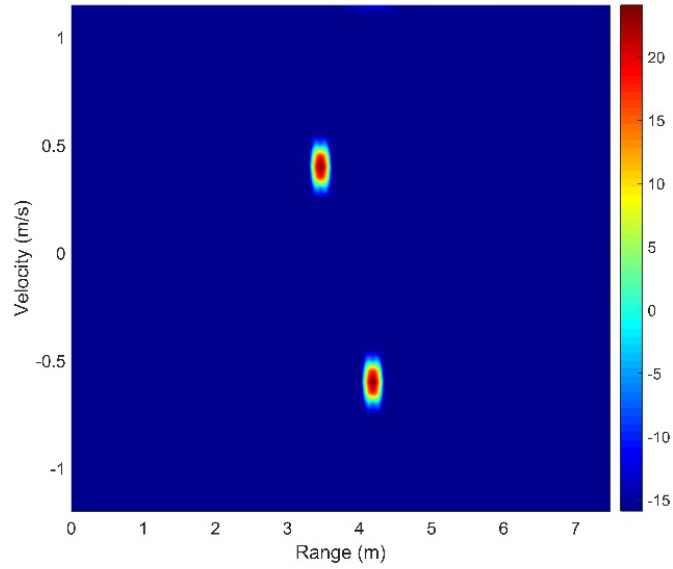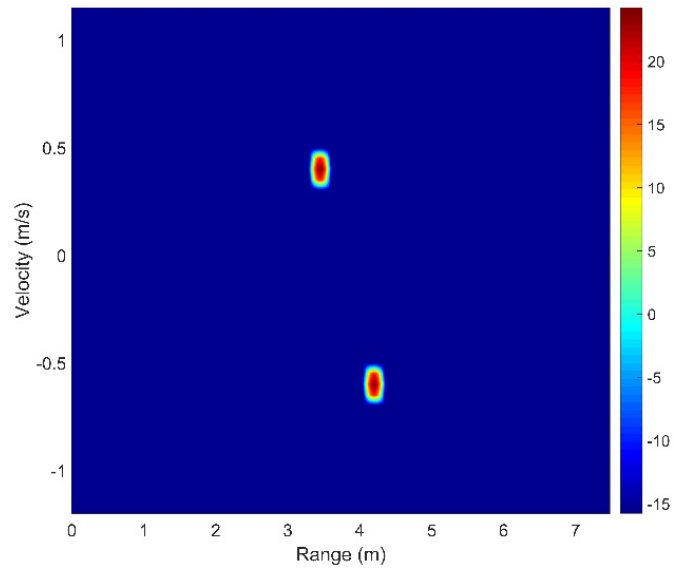

Fig. 7   **R/D map of the 2 targets considered in the numerical example, obtained by the Keystone transform method, for a 1.2-s CPI centered at** t **= 1.5 s. Cubic spline interpolation was used in the implementation of the Keystone transform.**

4. Discussion

4.1 Computational Aspects

In this section, we analyze the computational aspects of the various UWB Doppler processing schemes. As suggested by a comparison of Eqs. 6 and 7, the implementation of the exact matched filter should come at an increased complexity in computational terms, as compared to the conventional Doppler processing formula.

We assume that the radar data are already organized in a 2-D array of size M by N, $S(f_m, t_{sn})$, with the 2 dimensions representing frequency and slow time. Note that some UWB waveform implementations, such as stepped frequency or linear frequency modulation combined with stretch processing,[7] generate radar data directly in the frequency domain. For other types of waveforms, such as UWB impulses or pulse compression waveforms, the radar data are generated in the time domain and need to be transformed to the frequency domain via FFTs.

The conventional Doppler processing described by Eq. 7 is efficiently implemented as a 2-D FFT. The typical form of this algorithm is the row-column decomposition[4] and requires $O(MN \log_2 MN)$ floating-point operations (the symbol O stands for "on the order of"). When the radar data are directly available in the time domain, there is no need to convert to frequency domain in this Doppler processing scheme. Instead, the R/D map can be simply obtained by 1-D FFTs along the slow time dimension for each range bin, with a computational load of $O(MN \log_2 N)$. However, one should keep in mind that the difference between $O(MN \log_2 MN)$ and $O(MN \log_2 N)$ is smaller than it appears at first sight: when $M = N$, the difference is a factor of 2.

For the direct (or brute-force) matched filter implementation described by Eq. 6, we cannot apply FFT-like algorithms due to the shape of the support in the $\rho - u$ domain. Instead, one needs to compute the double sum in Eq. 6, pixel-by-pixel. Since there are MN pixels in an R/D map, and each pixel requires $O(MN)$ operations, the total computational load is $O(M^2 N^2)$, which is significantly larger than that required by the 2-D FFT algorithm. Note that the same load would be obtained if we implemented the 2-D DFT in Eq. 7 directly by double summation, instead of taking advantage of the efficiencies afforded by the FFT algorithm. When the original radar data are in the time domain, additional $O(MN \log_2 M)$ operations are required to convert them to the frequency domain via FFTs.

Another option for the direct matched filter implementation is to organize the data as a single-column vector of length MN, using the Kronecker product.[7] In that case, the R/D map is also organized as a vector of length MN, while the matched filter can be represented as an MN by MN matrix. The R/D map vector is then obtained by the matrix-vector multiplication of the matched filter with the radar data vector. The matrix-vector multiplication dictates a computational load of $O\left(M^2 N^2\right)$, same as the method described in the previous paragraph. However, this method is not particularly efficient in terms of computing resource usage due to the large storage size of the matched filter matrix, as well as the time required to compute its elements (as an example, for the parameters of the simulation in Section 3, the matrix would have a size of 1.66 GB). This approach could only be justified in a scenario where we must repeatedly apply the same matched filter to a stream of radar data, such as in creating a joint range-time-frequency representation (JRTFR)[1] where successive R/D maps obtained at different time intervals are stacked into a 3-D data structure.

The matched filter implemented via the Keystone transform is more efficient than the brute-force method, since it uses the 2-D FFT algorithm. As in the conventional Doppler processing, creating the R/D map requires only $O\left(MN \log_2 MN\right)$ operations, which represents significant savings versus the $O\left(M^2 N^2\right)$ operations required by the brute-force implementation. However, now we have to take into account the extra operations involved in the interpolation required by remapping the data samples. The additional computational load depends on the interpolation method employed; this can vary from $O(MN)$ for linear interpolation (which is simple but generally inadequate for this purpose) to $O\left(MN \log_2 N\right)$ for Fourier- (or sinc-) type interpolation. In the latter case, the data interpolation step approaches the load of the 2-D FFT itself, which means that it may represent a large part of the total computational time required by this method.

4.2 Range and Doppler Ambiguities

So far, we have not discussed the issue of ambiguities created by the range-Doppler processing of radar data. Since this is an important problem in the implementation of radar waveforms and processing schemes, this section analyzes it in detail. In particular, as suggested by Le Chevalier,[2] the UWB Doppler processing presented in this note may significantly reduce the Doppler ambiguities as compared to the conventional processing method. The derivation of the AF presented in this section confirms this fact in a quantitative way.

We start by analyzing the conventional (or narrowband, hence the subscript N) AF, as defined by Rihaczek.[8]

$$\chi_N(\tau, f_d) = \int_{-\infty}^{\infty} x(t)x^*(t-\tau)\exp(-j2\pi f_d t)dt. \tag{12}$$

When the radar waveform $x(t)$ consists of a train of baseband pulses, described as $x(t) = \sum_{n=0}^{N-1} p(t - nT_r)$, this function becomes

$$\chi_N(\tau, f_d) = \sum_{n=0}^{N-1} \int_{-\infty}^{\infty} x(t)p^*(t - nT_r - \tau)\exp(-j2\pi f_d t)dt. \tag{13}$$

A straightforward interpretation of this equation is that the AF represents the R/D map of a stationary ($v = 0$) point target placed at range $R = 0$, obtained by the conventional Doppler processing method. Equation 13 involves pulse compression, which corresponds to correlating the received signal with the transmitted pulse $p(t)$. However, as discussed in Section 2, our method of creating R/D maps omitted the pulse compression step by considering $p(t)$ as either a UWB impulse or the output of the pulse compression operation on the original transmitted waveform. A modified AF that more closely resembles the conventional Doppler processing scheme described in Section 2 is the following (note the superscript S for "simplified"):

$$\chi_N^S(\tau, f_d) = \sum_{n=0}^{N-1} \int_{-\infty}^{\infty} x(t)\delta(t - nT_r - \tau)\exp(-j2\pi f_d t)dt$$

$$= \exp(-j2\pi f_d \tau)\sum_{n=0}^{N-1} x(\tau + nT_r)\exp(-j2\pi f_d nT_r). \tag{14}$$

The only change in Eq. 14 as compared to Eq. 13 is replacing $p(t)$ inside the integral with a delta function $\delta(t)$. The second expression in Eq. 14 can be further analyzed by the methods developed by Rihaczek.[8] Letting $f_d = 0$, we obtain the expression $\sum_{n=0}^{N-1} x(t + nT_r)$, which describes N replicas of the original transmitted signal along the range axis, spaced apart by $\dfrac{cT_r}{2}$; these replicas generate the range ambiguities in the R/D map. These ambiguities are characteristic to any radar waveforms involving a periodic train of pulses.

In this work, we are more focused on analyzing the Doppler ambiguities obtained under the various processing schemes. To investigate these, we let $\tau = 0$ in Eq. 14 and write $x(t)$ explicitly as $\sum_{k=0}^{N-1} p(t - kT_r)$:

$$\left|\chi_N^S(0, f_d)\right| = \sum_{n=0}^{N-1}\sum_{k=0}^{N-1} p((n-k)T_r)\exp(-j2\pi f_d nT_r). \tag{15}$$

Since the duration of $p(t)$ is much smaller than T_r, the quantity under the double sum is nonzero only when $n = k$:

$$p((n-k)T_r) = \begin{cases} p(0) & \text{for } n = k \\ 0 & \text{for } n \neq k \end{cases}. \tag{16}$$

Consequently, we obtain

$$\left|\chi_N^S(0, f_d)\right| = \sum_{n=0}^{N-1} p(0)\exp(-j2\pi f_d nT_r) = p(0)\frac{\sin(\pi f_d NT_r)}{\sin(\pi f_d T_r)}. \tag{17}$$

The expression on the right-hand side of Eq. 17 is a form of the Dirichlet (or digital sinc) function, frequently encountered in digital signal processing involving DFTs. A plot of $\left|\chi_N^S(0, f_d)\right|$ (cut through the AF along the Doppler frequency axis), obtained for the simulation parameters in Section 3, is shown in Fig. 8. Notice the equal peaks of amplitude $Np(0)$, spaced apart by $\dfrac{1}{T_r}$; these peaks (also known as grating lobes) generate the Doppler ambiguities in the R/D maps obtained by conventional Doppler processing.
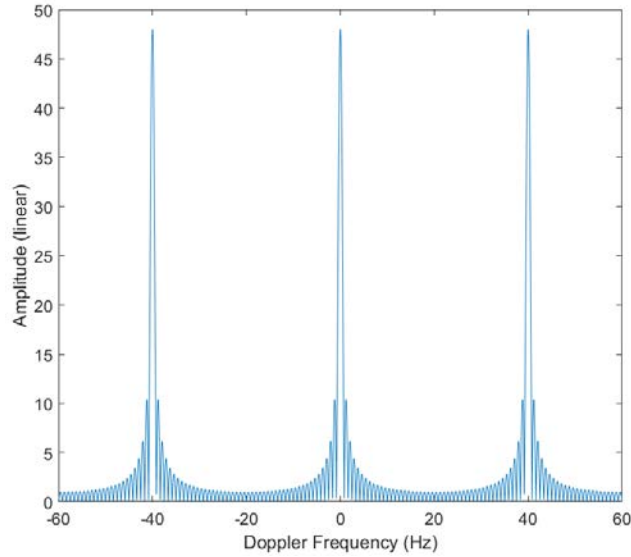

Fig. 8   Cut through the narrowband AF along the Doppler frequency axis, demonstrating the periodic Doppler ambiguities

While the AF definition in Eq. 12 is adequate for describing Doppler processing with narrowband waveforms, it does not capture all the phenomenology of sensing a moving target by a radar system operating with wideband waveforms. In order to account for the latter, we introduce the so-called "wideband AF",[9] defined as

$$\chi_W(\tau, f_d) = \int_{-\infty}^{\infty} x(t) x^* \left(t - \tau + \frac{f_d}{f_0} t \right) \exp(-j2\pi f_d t) dt .$$ (18)

For a train of baseband pulses $x(t) = \sum_{n=0}^{N-1} p(t - nT_r)$, we have

$$\chi_W(\tau, f_d) = \sum_{n=0}^{N-1} \int_{-\infty}^{\infty} x(t) p^* \left(t - nT_r - \tau + \frac{f_d}{f_0} t \right) \exp(-j2\pi f_d t) dt .$$ (19)

Change the integration variable to $t_f = t - nT_r$:

$$\chi_W(\tau, f_d)$$
$$= \sum_{n=0}^{N-1} \int_{-\infty}^{\infty} x(t_f + nT_r) p^* \left(t_f \left(1 + \frac{f_d}{f_0} \right) - \tau + \frac{f_d}{f_0} nT_r \right) \exp(-j2\pi f_d (t_f + nT_r)) dt_f$$
$$\cong \sum_{n=0}^{N-1} \exp(-j2\pi f_d nT_r) \int_{-\infty}^{\infty} x(t_f + nT_r) p^* \left(t_f - \tau + \frac{f_d}{f_0} nT_r \right) \exp(-j2\pi f_d t_f) dt_f .$$ (20)

Similarly to the narrowband AF analysis, we introduce a simplified version of the wideband AF, which closely reflects the "wideband" matched filter processing used in creating R/D maps with UWB waveforms (Eq. 6). This new AF is obtained by replacing $p(t)$ inside the integral with a delta function $\delta(t)$:

$$\chi_W^S(\tau, f_d)$$
$$= \sum_{n=0}^{N-1} \exp(-j2\pi f_d nT_r) \int_{-\infty}^{\infty} x(t_f + nT_r) \delta \left(t_f - \tau + \frac{f_d}{f_0} nT_r \right) \exp(-j2\pi f_d t_f) dt_f$$
$$\cong \exp(-j2\pi f_d \tau) \sum_{n=0}^{N-1} x \left(\tau + nT_r - \frac{f_d}{f_0} nT \right) \exp(-j2\pi f_d nT_r)$$ (21)

After replacing $x(t)$ by $\sum_{k=0}^{N-1} p(t - kT_r)$, we obtain

$$\left| \chi_W^S(\tau, f_d) \right| = \sum_{n=0}^{N-1} \sum_{k=0}^{N-1} p \left(\tau + (n-k)T_r - \frac{f_d}{f_0} nT_r \right) \exp(-j2\pi f_d nT_r).$$ (22)

By a similar argument as the one used in Eq. 16 and noting that $f_d \ll f_0$, we can write

$$p\left(\tau + (n-k)T_r - \frac{f_d}{f_0}nT_r\right) = \begin{cases} p(\tau) & \text{for } n = k \\ 0 & \text{for } n \neq k \end{cases}. \tag{23}$$

Consequently,

$$\left|\chi_W^S(\tau, f_d)\right| = \sum_{n=0}^{N-1} p\left(\tau - \frac{f_d}{f_0}nT_r\right)\exp\left(-j2\pi f_d nT_r\right). \tag{24}$$

Now let us write $p\left(\tau - \frac{f_d}{f_0}nT_r\right)$ as an inverse Fourier transform, using τ and f_m as the Fourier variable pair (note that f_m are discrete frequency samples):

$$p\left(\tau - \frac{f_d}{f_0}nT_r\right) = \sum_{m=0}^{M-1} P(f_m)\exp\left(j2\pi\left((f_m + f_0)\tau - f_m\frac{f_d}{f_0}nT_r\right)\right). \tag{25}$$

Then, the wideband AF can be written as

$$\left|\chi_W^S(\tau, f_d)\right| = \sum_{m=0}^{M-1}\sum_{n=0}^{N-1} P(f_m)\exp\left(j2\pi\left((f_m + f_0)\tau - \left(1 + \frac{f_m}{f_0}\right)f_d nT_r\right)\right). \tag{26}$$

We can interpret this form of the wideband AF as the output of the "wideband" matched filter (as in Eq. 6) for a stationary point target placed at $R = 0$. Thus, the response of this target can be written as

$$S_{PT}(f_m, t_{sn}, 0, 0) = P(f_m). \tag{27}$$

The R/D map generated by this response, as a function of τ and f_d, is (see Eq. 8)

$$RDM(\tau, f_d) = \sum_{m=0}^{M-1}\sum_{n=0}^{N-1} P(f_m)\exp\left(j2\pi\left((f_m + f_0)\tau - \left(1 + \frac{f_m}{f_0}\right)f_d t_{sn}\right)\right), \tag{28}$$

which is identical to the expression in Eq. 26 given the fact that $t_{sn} = nT_r$.

To investigate the Doppler ambiguities, we go back to Eq. 24 and take a cut through the AF along the Doppler frequency axis (or $\tau = 0$):

$$\left| \chi_W^S \left(0, f_d \right) \right| = \sum_{n=0}^{N-1} p\left(-\frac{f_d}{f_0} nT_r \right) \exp\left(- j2\pi f_d nT_r \right). \qquad (29)$$

It is clear that this function does not resemble the digital sinc obtained in the narrowband case. In fact, when we plot it as a function of f_d (again for the simulation parameters in Section 3), we obtain the graph in Fig. 9. Notice that the peaks (grating lobes) present at $f_d = \pm\frac{1}{T_r}$ are strongly attenuated with respect to the peak at $f_d = 0$. We quantify this attenuation by computing the ratio

$$\frac{\left| \chi_W^S \left(0, \frac{1}{T_r} \right) \right|}{\left| \chi_W^S \left(0,0 \right) \right|} = \frac{\sum_{n=0}^{N-1} p\left(-\frac{n}{f_0} \right)}{Np(0)}. \qquad (30)$$
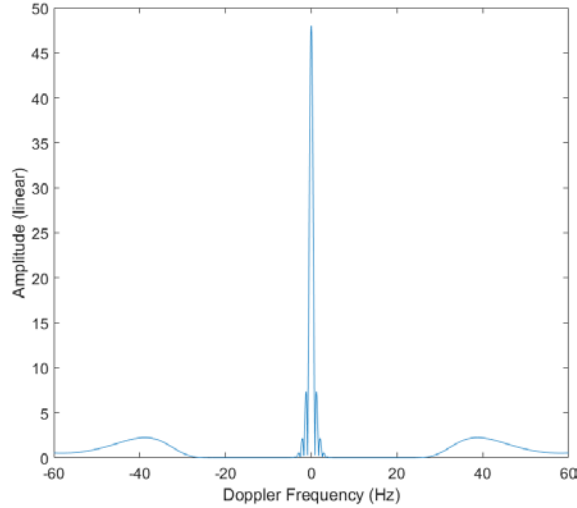

Fig. 9   Cut through the wideband AF along the Doppler frequency axis, demonstrating the attenuation of the Doppler ambiguities

Since $p(t)$ is monotonically decreasing away from $t = 0$, it follows that the ratio in Eq. 30 is always smaller than 1. Moreover, since $p(t)$ has a narrow support (typical for an UWB pulse), we expect $p\left(-\frac{n}{f_0} \right)$ to be zero for $n > N_1$, where N_1 is an integer smaller than N. Then the first grating lobe attenuation, or the ratio in Eq. 30, can be approximated by $\frac{N_1}{N}$. We can also establish an approximate relationship between N_1 and the pulse width of $p(t)$, denoted by τ_0: $\frac{N_1}{f_0} \cong \tau_0 \cong \frac{1}{B}$, where B is the pulse bandwidth.

18

The condition required to obtain a large attenuation of the first grating lobe is $\frac{N_1}{N} \ll 1$; by replacing N_1 with $\frac{f_0}{B}$ (or the inverse of the fractional bandwidth), we finally obtain $N \gg \frac{f_0}{B}$. This is identical to the formula indicated by Le Chevalier.[2] Translated in words, this formula says that the number of pulses in a CPI must be much larger than the inverse of the fractional bandwidth to achieve strong attenuation of the Doppler grating lobes in the wideband AF. This condition is relatively easy to satisfy for UWB pulses, which by definition have a large fractional bandwidth (or small $\frac{f_0}{B}$ ratio).

To clearly demonstrate the effect of the conventional and wideband Doppler processing schemes on the Doppler ambiguities, we revisit the numerical example in Section 3 by extending the velocity axis in the R/D maps to run from –2.4 to 2.4 m/s. Regardless of the processing scheme, both targets create an alias visible in these maps: the first target at –2 m/s and the second target at 1.8 m/s. However, the amplitude of these ambiguities differs dramatically between the conventional Doppler processing (Fig. 10), where they are as large as the true targets, and the wideband Doppler processing (Fig. 11), where they are strongly attenuated.
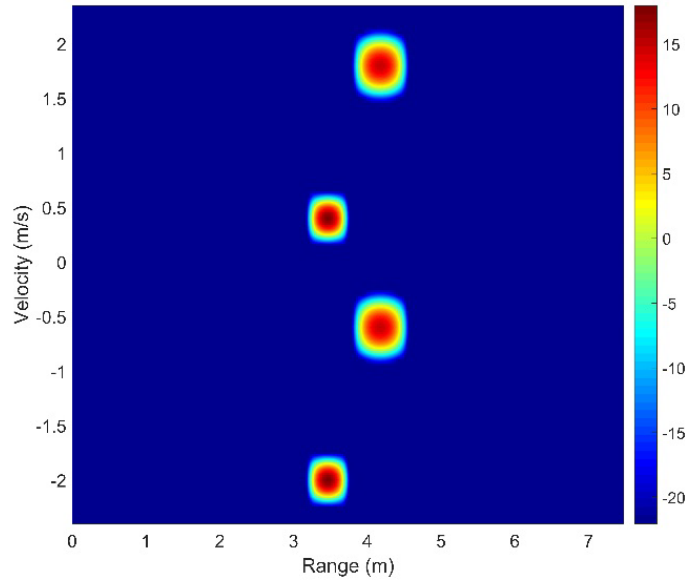

Fig. 10   R/D map of the 2 targets considered in the numerical example, obtained by conventional Doppler processing, showing an extended velocity scale to demonstrate the Doppler ambiguities
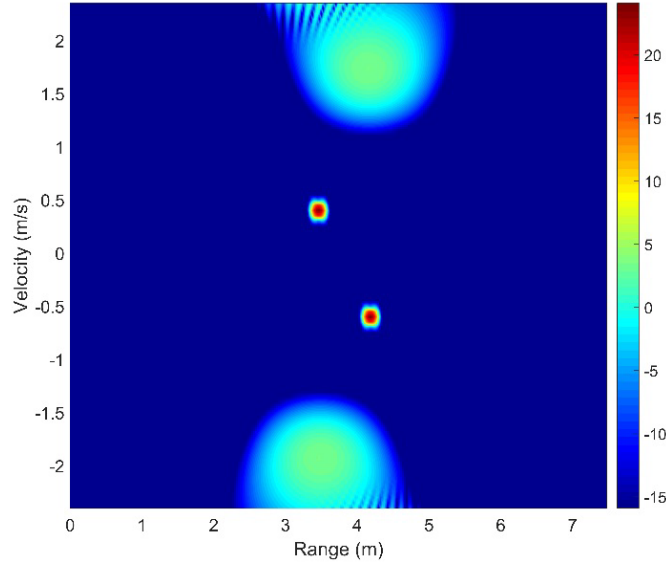
Fig. 11   R/D map of the 2 targets considered in the numerical example, obtained by the matched filter method, showing an extended velocity scale to demonstrate the Doppler ambiguities

The importance of this result in improving radar performance can be appreciated in the context of 2 traditional tradeoffs typically encountered in radar systems: 1) the tradeoff between range and Doppler resolutions[8] and 2) the tradeoff between range and Doppler ambiguities.[5] Thus, the shortcomings of the conventional Doppler processing proposed in our previous work[1] seemed to indicate that we cannot simultaneously increase the range and Doppler resolutions past certain limits by choosing both large signal bandwidth and long CPI duration due to the issue of target range migration within a CPI. However, these conflicting requirements are resolved through the wideband matched filter processing scheme. This allows us to choose a long CPI for good Doppler resolution, without limiting the signal bandwidth (which dictates the range resolution).

Regarding the tradeoff between range and Doppler ambiguities, this is dictated by the choice of PRF. In conventional Doppler processing, avoiding the grating lobes, which occur at intervals equal to PRF, typically requires a large PRF. On the other hand, avoiding the range ambiguities, which occur at intervals equal to $\dfrac{c}{2\text{PRF}}$, requires a small PRF. Several complex waveforms and signal processing techniques have been developed to mitigate this tradeoff[5,8] (e.g., transmission of trains of pulses with variable PRF), most of them involving additional penalties in system performance. Nevertheless, the processing scheme proposed in this note resolves this tradeoff by naturally suppressing the Doppler grating lobes as demonstrated in this section. Note that this effect holds only for the case of UWB waveforms (i.e., waveforms with large fractional bandwidth).

5. Conclusions

In this note, we presented a UWB radar Doppler processing scheme that overcomes the limitation reported in some of our previous work. The method is based on a careful derivation of the matched filter for this type of processing, taking into account the coupling between the frequency and slow time dimensions in the radar response of a point target. This coupling leads to a 2-D data transformation, similar to that employed in the formation of wideband, widebeam SAR images.

Theoretical and numerical comparisons of the new method with conventional Doppler processing clearly demonstrate the superior performance of the wideband matched filter in terms of both range and Doppler resolution, and at the same time explains why the old approach fails when UWB waveforms are employed. We also present an efficient implementation of the new technique, based on the Keystone transform, followed by a discussion of the computational complexity of all these processing schemes.

The detailed derivation of the wideband AF in Section 4.2 allowed us to confirm the result reported by Le Chevalier[2] regarding the mitigation of Doppler ambiguities by UWB waveforms. This is an important result showing that it is possible to resolve some traditional tradeoffs in radar system performance by using this type of waveform.

Regarding possible applications of this new Doppler processing method, one should mention the combination of micro-Doppler and high-range resolution analysis by means of the JRTFR. Given the good resolution in all dimensions (range, Doppler, and time), this type of analysis should be very beneficial to target classification problems. An excellent example of this processing applied to the analysis of a walking human target is presented by He et al.[3] We are confident that future investigations will reveal new applications of the wideband Doppler processing technique.

6. References

1. Dogaru T. Doppler processing with ultra-wideband (UWB) impulse radar. Adelphi (MD): Army Research Laboratory (US); 2013 Mar. Report No.: ARL-TN-0529.

2. Le Chevalier F. Wideband wide beam motion sensing. In: Taylor J, editor. Advanced ultrawideband radar: signals, targets, and applications. Boca Raton (FL): CRC Press; 2017. Chapter 12; p. 417–458.

3. He Y, Molchanov P, Sakamoto T, Aubry P, Le Chevalier F, Yarovoy A. Range-Doppler surface: a tool to analyze human target in ultra-wideband radar. IET Rad Sonar Nav. 2015;9(9):1240–1250.

4. Lim J. Two-dimensional signal and image processing. Upper Saddle River (NJ): Prentice Hall; 1990.

5. Richards M, Scheer J, Holm W. Principles of modern radar – basic principles. Raleigh (NC): SciTech Publishing; 2010.

6. Carrara W, Goodman R, Majewski R. Spotlight synthetic aperture radar. Norwood (MA): Artech; 1995.

7. Melvin W, Scheer J. Principles of modern radar – advanced techniques. Edison (NJ): SciTech Publishing; 2013.

8. Rihaczek A. Principles of high-resolution radar. New York (NY): McGraw-Hill; 1969.

9. Axelsson S. Noise radar using random phase and frequency modulation. IEEE Trans Geosci Rem Sens. 2004;42(11):2370–2384.

List of Symbols, Abbreviations, and Acronyms

1-D	1-dimensional
2-D	2-dimensional
3-D	3-dimensional
AF	ambiguity function
CPI	coherent processing interval
DFT	discrete Fourier transform
FFT	fast Fourier transform
I–Q	in-phase and quadrature
JRTFR	joint range-time-frequency representation
PRF	pulse repetition frequency
R/D	range-Doppler
SAR	synthetic aperture radar
UWB	ultra-wideband

1 (PDF)	DEFENSE TECHNICAL INFORMATION CTR DTIC OCA
2 (PDF)	DIR ARL IMAL HRA RECORDS MGMT RDRL DCL TECH LIB
1 (PDF)	GOVT PRINTG OFC A MALHOTRA
6 (PDF)	ARL RDRL SER U A SULLIVAN D LIAO T DOGARU K GALLAGHER B PHELAN RDRL SER W K RANNEY